Nanoscale

PAPER

View Article Online
View Journal

Cite this: DOI: 10.1039/d5nr03865k

Precise control of InP quantum dot growth *via* recyclable indium adducts

Ashleigh J. Cartlidge,†[a] Theodore A. Gazis,†[a,b] Ufedo-ojo Pitas,[a] Jasmine E. Robertson,[a] Lauren Matthews,[c] Martin J. Hollamby[a] and Peter D. Matthews*[a]

Received 12th September 2025,
Accepted 22nd December 2025

DOI: 10.1039/d5nr03865k

rsc.li/nanoscale

Indium phosphide is the most studied of the colloidal III–V QDs, with significant attention focused on the phosphorus source and/or reaction conditions to improve QD quality. Comparatively limited attention has been directed toward controlling the reactivity of the indium precursor. In this study we introduce an approach that utilizes recyclable triarylphosphine adducts of indium(III) chloride to selectively prepare InP QDs with absorption profiles spanning 419–620 nm. This control is achieved through careful choice of the triarylphosphine ligand, which changes the nature of the nucleation profile from continuous to burst.

Introduction

III–V Quantum Dots (QDs) are a class of nanoscale semiconductors that exhibit size-dependent band gaps and consist of a group 13 metal and a group 15 pnictogen. They hold significant potential in solution processed photonics, with applications in low energy lighting and displays and emerging use in light harvesting.[1–10] Amongst these, indium phosphide quantum dots offer an environmentally benign, and regulatory acceptable, alternative to their more toxic II-VI congeners, such as CdS, CdSe and PbS. InP-based light emitting diode (QD-LED) displays have been successfully commercialised by major manufacturers such as Samsung and LG.[11–13] The major challenge in realizing this potential lies in achieving precise control over the size of InP QDs to allow for targeted band gap sizes, and thus colour. Poor size control leads to size dispersity, which manifests as inhomogeneous spectral broadening, leading to poor device performance.[14–16]

In an ideal QD synthetic protocol, precursors first form a reservoir of monomeric species, which nucleate upon reaching a critical concentration, followed by a separate growth phase. The temporal separation between nucleation and growth is key to producing monodisperse size distribution, with final QD size dictated by the reaction duration.

Where colloidal InP QDs are concerned, these species are typically prepared *via* hot-injection of a phosphorus precursor, most commonly [$P(SiMe_3)_3$ or $P(NEt_2)_3$], into a high boiling point solvent containing either a long chain indium carboxylate or an indium halide.[11,14,15,17] The twin contributions of highly reactive precursors and strongly covalent In–P bonds make it difficult to control nanocrystal formation, which leads to irreproducible results, poor quality QDs and wide absorption/emission peaks.

Several strategies have been developed to achieve the temporal separation in InP QD systems, the majority of which have focussed on the phosphorus precursor.[17] Variants explored include $P(SiMe_3)_3$, $P(SiAr_3)_3$,[18] Ph_2PSiMe_3,[19] $P(GeMe_3)_3$,[20] PH_3,[21] P_4,[22] and modified reaction systems such as $P(SiMe_3)_3$ with a zinc complex,[23] controlled precursor addition through syringe pumps,[24] and tubular flow systems.[25] Perhaps the most promising advance has been the more radical shift from P(−III) to P(+III) sources, specifically tris(dialkylamino) phosphines.[26–29] These precursors are easy to handle and offer

[a]School of Chemical & Physical Sciences, Keele University, Newcastle-under-Lyme, ST5 5BG, UK. E-mail: p.d.matthews@keele.ac.uk
[b]Department of Chemistry, Materials, and Chemical Engineering "Giulio Natta", Politecnico di Milano, Piazza Leonardo da Vinci 32, IT-20133 Milano, Italy
[c]ISIS Pulsed Neutron Source, Rutherford Appleton Laboratory, Didcot, OX11 0QX, UK
†These authors contributed equally.

Peter D. Matthews

Peter Matthews is a Senior Lecturer in Inorganic & Materials Chemistry at Keele University, UK. He received his PhD in 2016 from the University of Cambridge, before moving to the University of Manchester as an EPSRC Doctoral Prize Fellow. In 2017, Peter moved to Keele University as a Research Fellow, and was appointed Lecturer in 2023. His research focus is on the synthesis and design of nanomaterials for Quantum 2.0.

excellent reproducibility, characteristics not shared with the historically used $P(SiMe_3)_3$. Notably, aminophosphines enable continuous rather than burst nucleation, which continues throughout the course of the reaction.[29]

In contrast, there have been relatively few attempts to control InP growth by tailoring the nature of the indium source. In $P(SiMe_3)_3$-based syntheses, the archetypal indium source is an indium(III) carboxylate, typically prepared *in situ* from $In(OAc)_3$ and a long chain carboxylic acid (*e.g.* myristic-, oleic-, palmitic acid).[30,31] For $P(NR_2)_3$ systems, indium(III) halides, particularly $InCl_3$, are the choice du jour,[14,17,32] with only limited exploration of alternatives such as $InBr_3$,[33] InI_3[34,35] or indium(I) halides.[36] Notably, the identity of the halide influences the optoelectronic properties of the QD. In a recent alternative approach, Larson and Cossairt employed ethylenediaminetetraacetic acid (EDTA) as a chelating ligand for $InCl_3$, reporting size-tuneable InP QDs ranging from 4.5–2.3 nm, and corresponding Lowest Energy Excitonic Transitions (LEETs) spanning 510–590 nm.[37]

An intriguing yet unexplored class of potential precursors are oxygen-free adducts of indium halides, particularly those involving triarylphosphines, which have a well-documented coordination chemistry.[38–40] Despite their known stability and well-characterized chemical behaviour, their potential in controlling InP QD synthesis remains underdeveloped, with no documented reports to the best of our knowledge. In this paper we address this gap and report on the use of oxygen free adducts of indium chloride, by utilising triarylphosphine adducts of $InCl_3$ as novel indium precursors. By judicious selection of the triarylphosphine ligand and reaction time we demonstrate precise and reproducible control over the QD LEETs from 419–620 nm, consistently yielding narrow full-width half maximums (FWHM). Importantly, upon completion of the QD synthesis, the triarylphosphine ligands can be efficiently isolated by simple crystallisation, offering an avenue for reusability that is typically limited in nanocrystal growth. This approach thus represents a versatile and sustainable pathway to high-quality InP QDs.

Experimental

Synthesis of triarylphosphine indium chloride adducts

Adapted from literature procedures.[40] Briefly, a solution of $InCl_3$ in ethyl acetate was added to a stoichiometric amount of the triarylphosphine, also in ethyl acetate. Over the course of an hour a white precipitate forms, which was collected and dried *in vacuo*. Compounds were checked for purity using elemental analysis and comparing the PXRD patterns against that calculated from known single-crystal X-ray diffraction data (SI S2).

Synthesis of InP QDs

Adapted from previous procedures.[37] In a nitrogen filled glovebox, the indium source (0.29 mmol) was suspended in oleylamine (5 mL) and then transferred to a Schlenk line. The solution was heated under dynamic vacuum at 120 °C for 1 h, backfilled with N_2 and then heated to 180 °C. After the temperature equilibrated, $P(NEt_2)_3$ (0.33 mL, 1.2 mmol) was rapidly injected. The reaction was monitored by taking 20 μL aliquots and dissolving them in spectroscopic grade toluene (2 mL). The reaction was monitored for 2 h, then cooled to room temperature. The QDs were precipitated with anhydrous methanol, centrifuged to 8 min at 3500 rcf and resuspended in anhydrous toluene. This was repeated 3 times.

Results and discussion

A reproducible and optimised protocol for the use of aminophosphines in InP QD synthesis is well established.[41] To ensure direct comparability with existing literature, we elected to employ this approach in our study. To this end, 1 eq. of indium precursor was heated in oleylamine under dynamic vacuum at 120 °C for 1 hour, backfilled with N_2 and then heated to 180 °C prior to the injection of 4 eq. of $P(NEt_2)_3$ (Scheme 1).

We monitored the progression of the system over a 2-hour period by withdrawing 20 μL aliquots at regular intervals. Each system was studied in at least triplicate to ensure reproducibility. In control experiments using $InCl_3$, we observed the expected progressive bathochromic shift in LEET (Fig. 1a), with a final absorbance at 607 ± 4 nm after 2 hours, consistent with literature precedents.[26,27,41]

Armed with a baseline, we replaced $InCl_3$ with $(Ph_3P)_2InCl_3$ (**1**), a trigonal bipyramidal complex with axial phosphine ligands (SI Fig. S1).[38–40] We posited that the electron-donating Lewis basic phosphine ligands in (**1**) would weaken the In–Cl bonds and increase chloride lability, leading to an enhanced precursor reactivity and so form InP-monomers at a faster rate.

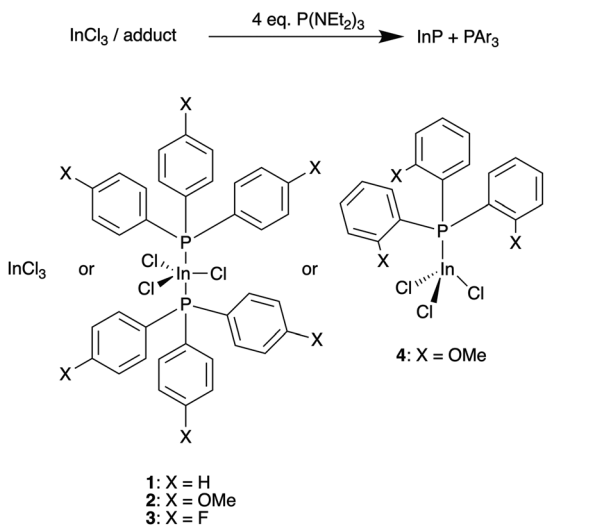

Scheme 1 Reaction scheme for the formation of InP QDs used in this report.

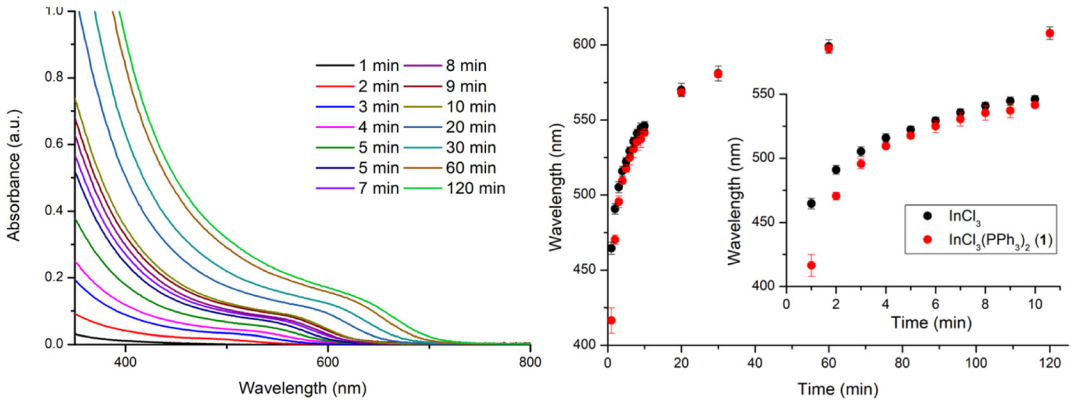

Fig. 1 (a) UV-vis spectra monitoring the growth of InP prepared using $(Ph_3P)_2InCl_3$ (**1**) and (b) change in the lowest energy excitonic transition (LEET) over the course of the reaction when using $InCl_3$ or **1** as the indium source.

In the nucleation and growth of InP QDs, the first step is the formation of InP-monomers and when these hit a critical concentration nucleation occurs. For $P(NR_2)_3$ systems that undergo a continuous nucleation system, the slow formation of monomers leads to a long nucleation period, shorter growth periods and thus results in small QDs. On the other hand, fast monomer formation results in a shorter nucleation period, extended growth and thus larger QDs. For a burst nucleation system, the reverse would be true: fast initial rate leads to a large number of nuclei with limited monomer amounts left for growth, whereas a slow initial rate allows a large monomer reservoir for extended growth leading to large QDs.[37] Here we determined the reaction rate by calculating the concentration of InP using the high energy absorbance attributed to bulk InP (SI section S6),[27,29,37] which is really the growth rate of crystalline InP and not the monomer production rate.

$(Ph_3P)_2InCl_3$ (**1**) produced InP at a slower initial rate (2.95 mM min^{-1}) than $InCl_3$, (3.67 mM min^{-1}) (Table 1). Alongside a lower InP concentration in the initial 4 minutes for **1** (SI Fig. S21–S25), the QDs prepared from **1** displayed more LEETs with a greater hypsochromic shift and thus smaller QDs. This runs in agreement to the expected behaviour, where the slower rate of monomer formation result in a longer nucleation period and thus shorter growth – giving rise to smaller QDs. We tested whether it was necessary to preform the adduct by using an appropriate 2 : 1 ratio of PPh_3 and $InCl_3$ as the indium source and observed behaviour that was quite closely aligned to that with $InCl_3$ (SI Fig. S15), suggesting the adducts are important.

Table 1 Initial rates of InP formation, measured over the first 4 minutes of the reaction from the [InP]

Indium source	Initial rate/mM min^{-1}
$InCl_3$	3.67
$(PPh_3)_2InCl_3$ (**1**)	2.95
$[P(4\text{-}MeOC_6H_5)_3]_2InCl_3$ (**2**)	2.76
$[P(4\text{-}FC_6H_4)_3]_2InCl_3$ (**3**)	3.75
$[P(2\text{-}MeOC_6H_4)_3]InCl_3$ (**4**)	2.68

To probe the effect of the precursors further, we conducted mixed-precursor experiments using combinations of **1** and $InCl_3$, whilst maintaining a constant total molar concentration of indium. During the first 10 minutes, increasing the amount of **1** causes a hypsochromic shift of the LEET relative to $InCl_3$, suggesting smaller QDs (Fig. 2 and SI Fig. S14). For the reaction rates there are two trends at play: from 25–75% **1** there is a decrease in initial rate, corresponding to a hypsochromic shift in LEET, however at 100% **1** the initial rate jumps slightly (SI Table S2, Fig. S25 and S26). This behaviour suggests that the different precursors contribute to the nucleation and growth periods in different manners, leading to the intriguing possibility of switching between continuous and burst nucleation through choice of precursor.

Motivated by this result, we explored the effect of ligand basicity using more and less electron-rich phosphine derivatives. We prepared a selection of triarylphosphine adducts of $InCl_3$ following established protocols that combine solutions of $InCl_3$ and the relevant phosphine in ethyl acetate, from which the adduct precipitates.[40] Specifically, we employed tris

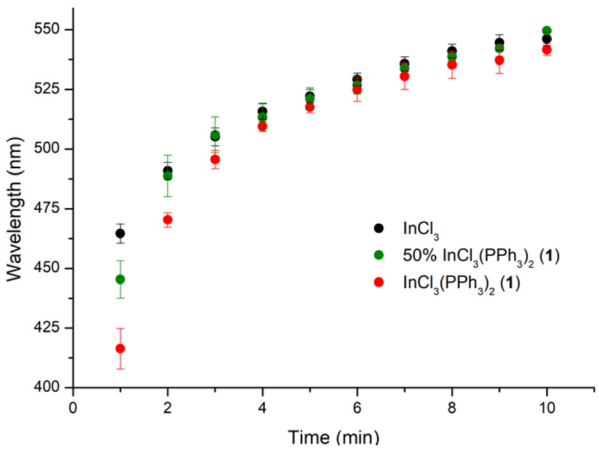

Fig. 2 Behaviour of the LEET for QDs prepared from differing ratios of $InCl_3$ to $(Ph_3P)_2InCl_3$ (**1**).

(4-methoxyphenyl)phosphine and tris(4-fluorophenyl)phosphine to prepare the corresponding 2 : 1 adducts with $InCl_3$: [P(4-$MeOC_6H_5$)$_3$]$_2InCl_3$ (**2**, SI Fig. S2) and [P(4-FC_6H_4)$_3$]$_2InCl_3$ (**3**), respectively. Like (**1**), these complexes adopt a 2 : 1 trigonal bipyramidal structure with axial phosphine coordination. All three species possess identical cone angles (145°),[42] ensuring comparable steric environments around the In centre. However, their basicities differ markedly, with pK_a values of 4.57 for P(4-$MeOC_6H_5$)$_3$, 2.73 for Ph_3P and 1.97 for P(4-FC_6H_4)$_3$,[43] which should impact the triarylphosphine-In bond strength. Indeed, reported single crystal X-ray analysis revealed In–P bond lengths of 2.868 Å for **2** and 2.697–2.729 Å for **3** (SI Table S1).[40]

The influence of the phosphine ligand basicity is evident in the rate of bathochromic shift for the LEET during the course of the reaction (Fig. 3 and SI Fig. S4–S8). After 2 minutes, the control ($InCl_3$ only) stands at 491 ± 3 nm, whilst the adducts vary from 470 ± 3 nm (**1**) to 489 ± 2 nm (**2**) and 450 ± 8 nm (**3**). By 4 minutes the LEETS of the more reactive adducts have a continued their bathochromic shift to 509 ± 2 nm (**1**), 520 ± 6 nm (**2**) and 491 ± 3 nm (**3**) in comparison to $InCl_3$ (516 ± 3 nm). Interestingly **2** has a much slower reaction rate than **3** (Table 1 and SI Fig. S21–S24), demonstrating the impact of the electron donating methoxy group *versus* the electron withdrawing fluoride. Despite **3** having the fastest rate, it has the smallest LEETs, which is contrary to the expected behaviour, and indicates that the reduced growth must be due to a switch to the burst nucleation regime.

To probe precursor control beyond electronic influences, we explored steric effects using tris(2-methoxyphenyl)phosphine, which forms a 1 : 1 tetrahedral coordination complex with indium chloride owing to the increased cone angle (176°).[44,45] The resulting complex, [P(2-$MeOC_6H_4$)$_3$]$InCl_3$ (**4**, SI Fig. S3) features a shorter In–P bond of 2.543 Å may also contribute to the observed behaviour. Regardless, (**4**) exhibits a substantially slower initial reaction rate among all precursors examined (Table 1), with a LEET of 456 ± 11 nm at 2 minutes, red-shifting to 482 ± 11 nm after 4 min (Fig. 2). Notably, these values also show a hypsochromic shift relative to the $InCl_3$ only control, indicating that judicious choice of the electronic (**2** and **3**) or steric (**4**) environment of the triarylphoshpine can either promote or supress early-stage QD growth.

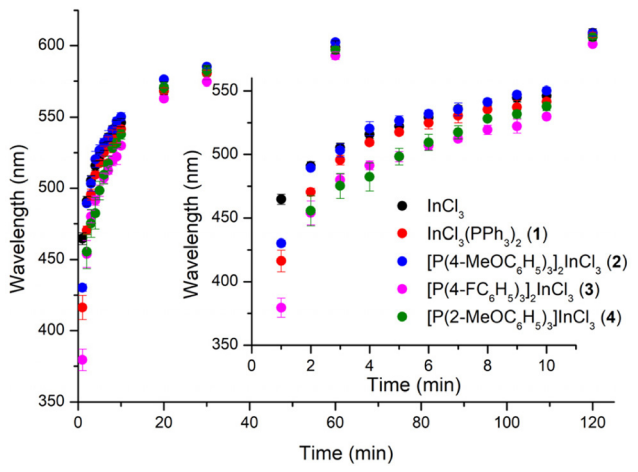

Fig. 3 Behaviour of the LEET for QDs prepared from $InCl_3$ (blue), $(Ph_3P)_2InCl_3$ (**1**, orange), [P(4-$MeOC_6H_5$)$_3$]$_2InCl_3$ (**2**, green), [P(4-FC_6H_4)$_3$]$_2InCl_3$ (**3**, red) and [P(2-$MeOC_6H_4$)$_3$]$InCl_3$ (**4**, purple).

These outcomes are further evident when calculating the yield of the InP QDs (SI Fig. S27–S30). The yields of all the precursors approached a similar ending point, but there is reasonable deviation in the first 10 minutes. The yield of InP when using both $InCl_3$ and **3** outpaces the other indium precursors, mirroring the initial rates of reaction. When using the different ratios of **1** : $InCl_3$, we observe the same trend as previously with the yields of InP decreasing with increasing amounts of **1**, before switching to a much higher amount with 100% **1**.

The LEETs of all reactions displayed a progressive bathochromic shift during the course of the reaction following a trend that could be fitted to a power law (SI Fig. S4–S8). After approximately 2 hours, the bathochromic shift plateaued across all systems, converging toward a final LEET in the 600–620 nm range. Concurrently, the full width half maxima (FWHM) for each set of reaction conditions improves from 0.28 eV to 0.13 eV, with limited differences between each of the different adducts (SI Fig. S13). Interestingly the improvement in FWHM tended to plateau after about 20 minutes, indicating limited size focusing effects in the latter stages of the reaction. Together, these observations suggest that the role of the precursors is key in the early stages of the reaction, but limited in the latter growth period of the QDs.

Since our systems follow a power law model, we postulated that we could accurately target specific QD LEETs in the 419–620 nm range by careful selection of time and precursor adduct, with major differentiation in the early stages of the reaction. We ran reactions for a range of the precursors and stopped them at different time points. Pleasingly, we found that we could achieve results within two standard errors of the predicted wavelength for a chosen reaction time and precursor, demonstrating the viability of this approach (SI Fig. S9–S12).

With a detailed understanding of the optoelectronic properties of the QDs in hand, we next investigated their physical attributes. High-angle annular dark-field scanning transmission electron microscopy (HAADF-STEM) confirmed that all of QDs adopt the expected tetrahedral shape that is characteristic of InP QDs prepared using aminophosphine (SI Fig. S31–S35).[46]

To gain insight into the QD sizes in solution, small-angle scattering data, using both X-rays (SAXS) and neutrons (SANS) as the incident radiation was collected. Fig. 4 shows the resulting scattering profiles for InP QDs formed using PPh_3 and 2-$MeOC_6H_4$ ligands. Profiles for InP QDs formed using other ligands are provided in the SI (SI Fig. S37). All datasets exhibit a power-law decay in intensity at low Q, characteristic of a loosely aggregated floc of small particles, with features in the mid-high Q range that are likely to arise from the form of the QDs themselves.

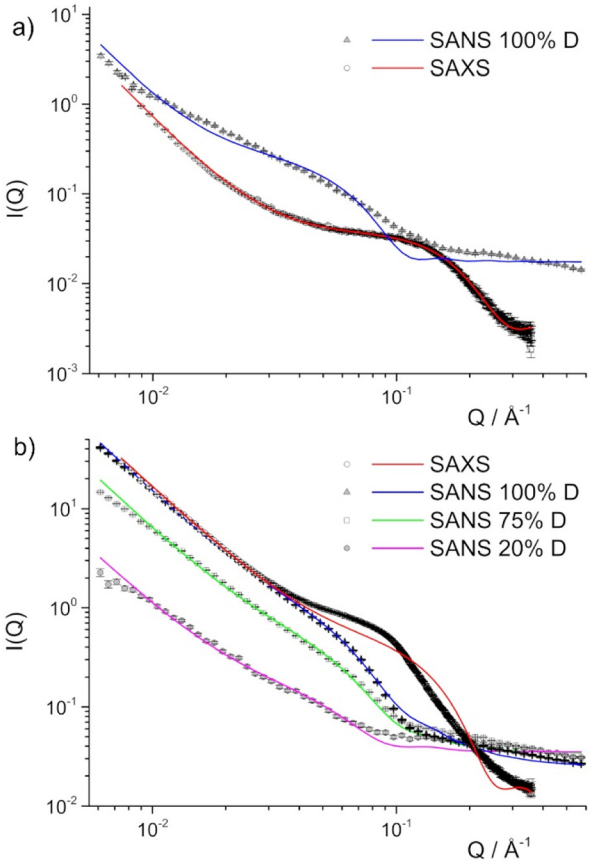

Fig. 4 SANS and SAXS data for InP QDs formed using (a) $(PPh_3)_2InCl_3$ and (b) $[P(2\text{-}MeOC_6H_4)_3]InCl_3$ precursors. Lines are model fits to the data using a method as outlined in the text. SAXS data was collected using toluene-d8 as the solvent. In panel (b), contrast-variation SANS data was collected in mixtures of toluene-d8 and toluene h8. The "% D" in the legend indicates the %vol of toluene-d8 in that mixture.

Analysis of all SAXS and SANS data was carried out in SasView[47] using a model describing a population of core–shell spheres, an additional power law to describe the aggregates and a flat background. An InP QD core surrounded by an oleylamine shell was assumed. The use of a spherical model is an approximation but is a reasonable one due to averaging from rotation during the SANS measurement. Taking this into account, it is likely that the resulting parameters capture the size of the central part of the tetrahedron, as suggested schematically in SI Fig. S37. Global fitting with constrained parameters was applied – *i.e.* for the example of PPh_3 in Fig. 4a, both SAXS and SANS data was analysed using shared core radius, shell width and power law exponent. More detail on data analysis can be found in the supplementary methods section in the SI S9. Fit results for the core radii and power law exponents are provided in Table 2. As can be seen, there is little difference between the InP QDs dispersions prepared using the different ligands, which fits the UV spectra where there is limited differentiation after two hours of growth.

To complement our structural characterization and gain insight into the fate of the triarylphosphines post QD synthesis, we subjected QDs prepared using **3** to ^{31}P and ^{19}F NMR spectroscopy (SI Fig. S16 and S17). We were particularly interested in determining whether any triarylphosphines were coordinated to the surface of the QDs. Free $P(4\text{-}FC_6H_4)_3$ was observed in reaction aliquots, but both measurements showed no evidence for the inclusion of triarylphosphines in the purified QDs. This indicates that the observed differences in UV-vis spectra arise from QD size rather than surface-bound triarylphosphine ligands. Consistent with these findings, energy dispersive X-ray (EDX) and X-ray photoelectron (XPS) spectra of QDs prepared from **3** showed no detectable fluorine, indicating no surface binding of $P(4\text{-}FC_6H_4)_3$ (SI Fig. S36).

Table 2 InP QD core radii and power law exponents obtained from analysis of contrast-variation SANS and SAXS data. Analysis errors on radii values are ± 0.1 nm, and ± 0.1 on power law exponents

Indium source	R_{core}/nm	Power law exponent
$InCl_3$	1.7	2.3
$(PPh_3)_2InCl_3$ (**1**)	1.4	2.8
$[P(4\text{-}MeOC_6H_5)_3]_2InCl_3$ (**2**)	1.6	2.0
$[P(4\text{-}FC_6H_4)_3]_2InCl_3$ (**3**)	1.7[a]	2.3
$[P(2\text{-}MeOC_6H_4)_3]InCl_3$ (**4**)	1.9	2.3

[a] This value was fixed in analysis due to a lack of available data for fitting.

Since the triarylphosphines were not incorporated into the QD surface, we considered two possibilities: (a) they decomposed at high temperatures into various by-products or (b) they were released intact and could be recovered and reused. To evaluate this, we monitored aliquots of a reaction involving **3** by ^{31}P NMR spectroscopy at regular intervals (SI Fig. S19). The signal corresponding to free $P(4\text{-}FC_6H_4)_3$ increased rapidly during the first stage of the reaction before plateauing. We referenced against an internal standard added to the NMR tube to determine the relative ratio of the formation of aminophosphonium cationic by-product (SI Fig. S20), which is produced at a slower rate.[37,41] This behaviour supports the conclusion drawn from the mixed-concentration experiments of **1** (Fig. 3) that the adducts play a key role in the nucleation phase, while subsequent InP QD growth follows a trajectory consistent with conventional aminophosphine pathways. An additional point to note is that by using a P-based ligand to vary the indium source's reactivity, we have avoided the presence of oxides that have been since with other O-based ligand systems.[37]

It was evident that a considerable amount of arylphoshpine was released during QD formation. To quantify this, the QDs were purified by methanol-induced precipitation followed by centrifugation. ^{31}P NMR spectra of the resulting supernatants from reactions involving complex (**1**) (SI Fig. S18) confirmed the presence of substantial free PPh_3. Notably, upon standing, the initial supernatant yielded crystalline PPh_3, which was subsequently isolated with a high recovery of 90% relative to the original amount used. These results conclusively show that triarylphosphines are neither retained within nor bound to the QD surface and the differences in QDs are thus not from

surface bound ligands. Critically, the efficient recovery of triarylphosphines opens up the potential for their reuse, suggesting a protocol that not only reliably synthesizes InP QDs of a targeted size but is also sustainable and economically advantageous.

Conclusions

Here we have demonstrated the ability to control InP QD size through the use of triarylphosphine adducts of indium chloride. This study shows that it is possible to influence the nucleation stage of the reaction by varying the reactivity of the indium precursor, and opens the door to intriguing possibilities of using bulkier or chelating phosphine ligands to really restrict the reactivity. The cone angles and basicity of the triarylphosphine are amongst the key factors that determine the resultant size of the QD, and this allows for the selective targeting of specific sizes of QD. We have shown that we are able to specifically target InP QDs that absorb from 419–620 nm through the selection of appropriate, repeatable conditions.

Author contributions

AJC: investigation, data curation, formal analysis. TAG: conceptualisation, investigation, data curation, formal analysis. UP: investigation, data curation, formal analysis. JER: investigation. LM: investigation, data curation, formal analysis. MJH: investigation, data curation, formal analysis. PDM: conceptualisation, funding acquisition, data curation, formal analysis, writing.

Conflicts of interest

There are no conflicts to declare.

Data availability

The raw and analysed data for this work is available from Keele University's Data Repository at: https://doi.org/10.21252/4z2v-rv91.

Supplementary information (SI): UV-vis spectra, NMR spectra, calculations, TEM images, XPS spectra and SANS/SAXS data. See DOI: https://doi.org/10.1039/d5nr03865k.

Acknowledgements

The authors acknowledge the support of EPSRC grants EP/V043412/1 (TAG, PDM) and UKRI649 (PDM), Keele University (AJC), Leverhulme Trust grant RPG-2024-416 (JER, PDM) and the UK Government and European Union as contributors to the Smart Energy Network Demonstrator, ERDF project number 32R16P00706 (PDM) for funding. This work was supported by the Henry Royce Institute for Advanced Materials, funded through EPSRC grants EP/R00661X/1, EP/S019367/1, EP/P025021/1 and EP/P025498/1. STFC are thanked for their support of the SANS and SAXS measurements at ISIS, UK on the SANS2D beamline *via* proposal RB2420416. This work benefited from the use of the SasView application, originally developed under NSF award DMR-0520547. SasView contains code developed with funding from the European Union's Horizon 2020 research and innovation programme under the SINE2020 project, grant agreement No. 654000.

References

1 B. Chen, D. Li and F. Wang, *Small*, 2020, **16**, 2002454.
2 E. Jang, Y. Kim, Y.-H. Won, H. Jang and S.-M. Choi, *ACS Energy Lett.*, 2020, **5**, 1316–1327.
3 T. Kim, K. H. Kim, S. Kim, S. M. Choi, H. Jang, H. K. Seo, H. Lee, D. Y. Chung and E. Jang, *Nature*, 2020, **586**, 385–389.
4 Z. Wu, P. Liu, W. Zhang, K. Wang and X. W. Sun, *ACS Energy Lett.*, 2020, **5**, 1095–1106.
5 W.-C. Chao, T.-H. Chiang, Y.-C. Liu, Z.-X. Huang, C.-C. Liao, C.-H. Chu, C.-H. Wang, H.-W. Tseng, W.-Y. Hung and P.-T. Chou, *Commun. Mater.*, 2021, **2**, 1–10.
6 W. Zhang, S. Ding, W. Zhuang, D. Wu, P. Liu, X. Qu, H. Liu, H. Yang, Z. Wu, K. Wang and X. W. Sun, *Adv. Funct. Mater.*, 2020, **30**, 2005303.
7 R. W. Crisp, N. Kirkwood, G. Grimaldi, S. Kinge, L. D. A. Siebbeles and A. J. Houtepen, *ACS Appl. Energy Mater.*, 2018, **1**, 6569–6576.
8 H. B. Jalali, S. Sadeghi, I. B. D. Yuksel, A. Onal and S. Nizamoglu, *Nano Res.*, 2022, **15**, 4468–4489.
9 S. Yang, P. Zhao, X. Zhao, L. Qu and X. Lai, *J. Mater. Chem. A*, 2015, **3**, 21922–21929.
10 Z. Wang, K. D. Wegner, L. M. S. Stiegler, X. Zhou, A. Rezvani, A. S. Odungat, B. Apeleo Zubiri, M. Wu, E. Spiecker, J. Walter, U. Resch-Genger and D. Segets, *ACS Appl. Nano Mater.*, 2024, **7**, 24262–24273.
11 D. Rajan, B. Manoj, S. Krishna, A. Thomas and K. G. Thomas, *ACS Energy Lett.*, 2025, 3700–3728.
12 R. H. A. Omari, A. Kumar, A. F. Al-Hussainy, S. Mohammed, A. Sinha, S. Ray and H. Noorizadeh, *Environ. Sci.:Adv.*, 2025, **4**, 1553–1586.
13 H. Wang, L. Zhao, X. Bao, H. Yu, G. Zhang, T. Wang, X. Meng, S. Liu, X. Yuan and W. Xie, *ACS Photonics*, 2025, **12**, 1999–2006.
14 S. M. Click and S. J. Rosenthal, *Chem. Mater.*, 2023, **35**, 822–836.
15 S. Tamang, C. Lincheneau, Y. Hermans, S. Jeong and P. Reiss, *Chem. Mater.*, 2016, **28**, 2491–2506.
16 H. A. Nguyen, G. Dixon, F. Y. Dou, S. Gallagher, S. Gibbs, D. M. Ladd, E. Marino, J. C. Ondry, J. P. Shanahan, E. S. Vasileiadou, S. Barlow, D. R. Gamelin, D. S. Ginger, D. M. Jonas, M. G. Kanatzidis, S. R. Marder, D. Morton,

C. B. Murray, J. S. Owen, D. V. Talapin, M. F. Toney and B. M. Cossairt, *Chem. Rev.*, 2023, **123**, 7890–7952.
17 T. A. Gazis, A. J. Cartlidge and P. D. Matthews, *J. Mater. Chem. C*, 2023, **11**, 3926–3935.
18 D. C. Gary, B. A. Glassy and B. M. Cossairt, *Chem. Mater.*, 2014, **26**, 1734–1744.
19 T. A. Gazis and P. D. Matthews, *Chem. Commun.*, 2022, **58**, 13799–13802.
20 D. K. Harris and M. G. Bawendi, *J. Am. Chem. Soc.*, 2012, **134**, 20211–20213.
21 L. Li, M. Protière and P. Reiss, *Chem. Mater.*, 2008, **20**, 2621–2623.
22 E. Bang, Y. Choi, J. Cho, Y. H. Suh, H. W. Ban, J. S. Son and J. Park, *Chem. Mater.*, 2017, **29**, 4236–4243.
23 S. Koh, T. Eom, W. D. Kim, K. Lee, D. Lee, Y. K. Lee, H. Kim, W. K. Bae and D. C. Lee, *Chem. Mater.*, 2017, **29**, 6346–6355.
24 P. Ramasamy, K. J. Ko, J. W. Kang and J. S. Lee, *Chem. Mater.*, 2018, **30**, 3643–3647.
25 Z. Wang and D. Segets, *React. Chem. Eng.*, 2023, **8**, 316–322.
26 M. D. Tessier, K. De Nolf, D. Dupont, D. Sinnaeve, J. De Roo and Z. Hens, *J. Am. Chem. Soc.*, 2016, **138**, 5923–5929.
27 M. D. Tessier, D. Dupont, K. De Nolf, J. De Roo and Z. Hens, *Chem. Mater.*, 2015, **27**, 4893–4898.
28 G. Laufersky, S. Bradley, E. Frécaut, M. Lein and T. Nann, *Nanoscale*, 2018, **10**, 8752–8762.
29 B. M. McMurtry, K. Qian, J. K. Teglasi, A. K. Swarnakar and J. De Roo, *Chem. Mater.*, 2020, **32**, 4358–4368.
30 L. Angelé, S. Dreyfuss, B. Dubertret and N. Mézailles, *Inorg. Chem.*, 2021, **60**, 2271–2278.
31 S. Xu, S. Kumar and T. Nann, *J. Am. Chem. Soc.*, 2006, **128**, 1054–1055.
32 H. A. Nguyen, F. Y. Dou, N. Park, S. Wu and H. Sarsito.
33 S.-W. Choi, H.-M. Kim, S.-Y. Yoon, D.-Y. Jo, S.-K. Kim, Y. Kim, S. M. Park, Y.-J. Lee and H. Yang, *J. Mater. Chem. C*, 2022, **10**, 2213–2222.
34 M. E. Mundy, F. W. Eagle, K. E. Hughes, D. R. Gamelin and B. M. Cossairt, *ACS Mater. Lett.*, 2020, **2**, 576–581.
35 M. E. Mundy, D. Ung, N. L. Lai, E. P. Jahrman, G. T. Seidler and B. M. Cossairt, *Chem. Mater.*, 2018, **30**, 5373–5379.
36 R. Yadav, Y. Kwon, C. Rivaux, C. Saint-Pierre, W. L. Ling and P. Reiss, *J. Am. Chem. Soc.*, 2023, **145**, 5970–5981.
37 H. Larson and B. M. Cossairt, *Chem. Mater.*, 2023, **35**, 6152–6160.
38 A. J. Carty and D. G. Tuck, *J. Chem. Soc. A*, 1966, 1081–1087.
39 A. J. Carty, *Can. J. Chem.*, 1967, **45**, 345–351.
40 F. Chen, G. Ma, G. M. Bernard, R. G. Cavell, R. McDonald, M. J. Ferguson and R. E. Wasylishen, *J. Am. Chem. Soc.*, 2010, **132**, 5479–5493.
41 A. Buffard, S. Dreyfuss, B. Nadal, H. Heuclin, X. Xu, G. Patriarche, N. Mézailles and B. Dubertret, *Chem. Mater.*, 2016, **28**, 5925–5934.
42 J. A. Bilbrey, A. H. Kazez, J. Locklin and W. D. Allen, *J. Comput. Chem.*, 2013, **34**, 1189–1197.
43 T. Allman and R. G. Goel, *Can. J. Chem.*, 1982, **60**, 716–722.
44 N. A. Bell, S. J. Coles, M. B. Hursthouse, M. E. Light, K. A. Malik and R. Mansor, *Polyhedron*, 2000, **19**, 1719–1726.
45 P. J. C. Hausoul, A. N. Parvulescu, M. Lutz, A. L. Spek, P. C. A. Bruijnincx, B. M. Weckhuysen and R. J. M. Klein Gebbink, *Angew. Chem., Int. Ed.*, 2010, **49**, 7972–7975.
46 K. Kim, D. Yoo, H. Choi, S. Tamang, J. H. Ko, S. Kim, Y. H. Kim and S. Jeong, *Angew. Chem., Int. Ed.*, 2016, **55**, 3714–3718.
47 SasViewhttps://www.sasview.org/.